




**Raffaele Del Grande · Kristian Piscicchia  · Michael Cargnelli · Laura Fabbietti · Johann Marton · Paweł Moskal · Àngels Ramos · Alessandro Scordo · Diana Sirghi · Magdalena Skurzok · Oton Vazquez Doce · Sławomir Wycech · Johann Zmeskal · Paolo Branchini · Eryk Czerwinski · Veronica De Leo · Erika De Lucia · Alessandro Di Cicco · Eleonora Diociaiuti · Raffaella Donghia · Paolo Fermani · Salvatore Fiore · Matteo Martini · Elena Perez Del Rio · Andrea Selce · Michał Silarski · Catalina Curceanu**

## On the $K^-$ Absorptions in Light Nuclei by AMADEUS

Received: 3 September 2020 / Accepted: 4 December 2020 / Published online: 1 February 2021  
© The Author(s), under exclusive licence to Springer-Verlag GmbH, AT part of Springer Nature 2021

R. Del Grande · L. Fabbietti · O. Vazquez Doce  
Physik Department E62, Technische Universität München, 85748 Garching, Germany

R. Del Grande · K. Piscicchia · A. Scordo · D. Sirghi · M. Skurzok · E. De Lucia · E. Diociaiuti · R. Donghia · P. Fermani · M. Martini · C. Curceanu  
INFN - Laboratori Nazionali di Frascati, 00044 Frascati, Italy  
E-mail: raffaele.delgrande@lnf.infn.it

R. Del Grande · K. Piscicchia (✉)  
Centro Ricerche Enrico Fermi - Museo Storico della Fisica e Centro Studi e Ricerche “Enrico Fermi”, 00184 Rome, Italy  
E-mail: kristian.piscicchia@cref.it

M. Cargnelli · J. Marton · J. Zmeskal  
Stefan-Meyer-Institut für Subatomare Physik, 1090 Wien, Austria

L. Fabbietti · O. Vazquez Doce  
Excellence Cluster “Origin and Structure of the Universe”, 85748 Garching, Germany

P. Moskal · M. Skurzok · E. Czerwinski · M. I. Silarski  
Institute of Physics, Jagiellonian University, 30-348 Cracow, Poland

A. Ramos  
Departament de Física Quàntica i Astrofísica and Institut de Ciències del Cosmos, Universitat de Barcelona, 08028 Barcelona, Spain

S. Wycech  
National Centre for Nuclear Research, 02-093 Warsaw, Poland

P. Branchini · A. Di Cicco · V. De Leo · A. Selce · S. Fiore  
INFN Sezione di Roma Tre, Roma, Italy

V. De Leo · E. Perez Del Rio  
Dipartimento di Fisica dell’Università “Sapienza”, Roma, Italy

V. De Leo · S. Fiore · E. Perez Del Rio · A. Selce  
INFN Sezione di Roma, Roma, Italy

A. Di Cicco · A. Selce  
Dipartimento di Matematica e Fisica dell’Università “Roma Tre”, Roma, Italy

**Abstract** The aim of the AMADEUS collaboration is to provide experimental information on the low-energy strong interaction of antikaons with nucleons, exploiting the absorptions of low momentum  $K^-$  mesons ( $p_K \sim 127$  MeV/c) produced at the DAΦNE collider, in the materials composing the KLOE detector setup, used as an active target. The  $K^-$  single and multi-nucleon absorptions in light nuclei ( $^4\text{He}$  and  $^{12}\text{C}$ ) are investigated by reconstructing hyperon–pion, hyperon–nucleon/nucleus pairs, emitted in the final state of the reactions. In this paper the results obtained from the study of  $\Lambda\pi^-$ ,  $\Lambda p$  and  $\Lambda t$  correlated production are presented.

## 1 Introduction

We review the recent findings of the AMADEUS collaboration [1] concerning the low-momentum  $K^-$  interactions in light nuclear targets. The experiment exploits hadronic interactions of the  $K^-$  mesons produced at the DAΦNE [2] collider (with a mean momentum of  $p_K \sim 127$  MeV/c) with the materials of the KLOE detector [3]. The experimental study of hyperon resonances formation [4,5] and their behaviour in a nuclear environment [6,7], and the search for exotic  $K^-$  multi-nucleon bound states [8–18], is a fundamental input to the hadronic nuclear physics sector with strangeness  $S = -1$  to understand how the explicit and spontaneous chiral symmetry breaking occur in a nuclear medium.

The antikaon–nucleon ( $\bar{K}N$ ) strong interaction potential is attractive in the medium due to the existence of the  $\Lambda(1405)$  (isospin  $I = 0$ ) resonance in the energy region below the  $\bar{K}N$  threshold. In phenomenological potential models [19,20] the  $\Lambda(1405)$  is interpreted as a pure  $\bar{K}N$  bound state with a binding energy (BE) of about 27 MeV. According to the chiral unitary models [21–27] the  $\Lambda(1405)$  emerges from the interference of two poles, as a molecular meson-baryon state. The lower mass pole (about 1390 MeV) is mainly coupled to the  $\Sigma\pi$  decay channel, and the high mass pole, which is mainly coupled to the  $\bar{K}N$  channel, is located around 1420 MeV. The coupled-channel nature of the  $\bar{K}N$  interaction was recently confirmed by studying the  $K^-p$  correlation in pp collisions at the LHC measured by ALICE [28]. For this reason the shape of the measured  $(\Sigma\pi)^0$  invariant mass distribution is expected to change depending on the decay channel, due to the isospin interference term (which contributes with opposite sign to the  $\Sigma^\pm\pi^\mp$  cross sections, and vanishes for  $\Sigma^0\pi^0$ ) but also on the production channel. The experimental characterisation of the yield and spectral shape of the non-resonant antikaon–nucleon absorption below the  $\bar{K}N$  threshold, resulting in a hyperon–pion final state, is a good constraint for the chiral predictions (see e.g. [23]) since the real and imaginary parts of the calculated transition amplitudes are strongly model dependent in the sub-threshold region both in  $I = 0$  and  $I = 1$ . Moreover, it serves as a reference in the scenario which outlines the  $\bar{K}N$  channel as the golden production mechanism for investigating the high mass pole of the  $\Lambda(1405)$ . In particular, the modulus of the  $K^-n \rightarrow \Lambda\pi^-$  transition amplitude for the non-resonant ( $s$ -wave)  $\Lambda\pi^-$  production was measured in Ref. [29]. Comparison of this result with the recent theoretical findings is discussed in Sect. 4.

It was recently shown in Refs. [30,31] that  $K^-$ -nuclear optical potentials based on  $K^-N$  scattering amplitudes fail to reproduce the kaonic atoms data along the periodic table of the elements, unless a  $K^-$  multi-nucleon potential term is added. The  $K^-$  multi-nucleon interaction is treated in Refs. [30,31] by means of a phenomenological approach. An upgrade in the treatment of the  $K^-$  two-nucleon absorption ( $K^-2NA$ ) based on a microscopic description of the three body problem is given in Refs. [32,33]. Moreover the total  $K^-2NA$  branching ratio (BR) is also calculated in Ref. [33]. Such novel theoretical findings demand comparisons with new, high precision, experimental values of yields and low-energy cross sections for those rare  $K^-$  multi-nucleon interaction reactions which were never singled out in the available bubble chamber data. Furthermore the experimental search for exotic bound states of  $K^-$  with nucleons, whose existence is related to the strength of the  $K^-$ -nuclei interaction potential, cannot ignore a comprehensive characterisation of the  $K^-$  multi-nucleon absorption processes. In Ref. [34] it was demonstrated that in stopped  $K^-$  induced reactions with  $^{12}\text{C}$  nuclei the formation of the most fundamental  $K^-pp$  state overlaps with the  $K^-2NA$  process. In Sect. 5 we review the experimental results obtained by AMADEUS on the BRs and low-energy cross sections for the  $K^-$  two, three and four nucleon absorptions (2NA, 3NA and 4NA) in  $^4\text{He}$  and  $^{12}\text{C}$  nuclei (see also Refs. [15,34–36]).

---

S. Fiore

Department of Fusion and Technology for Nuclear Safety and Security, ENEA, Frascati, RM, Italy

M. Martini

Dipartimento di Scienze e Tecnologie applicate, Università “Guglielmo Marconi”, Roma, Italy

## 2 Experimental Apparatus

The DAΦNE (double annular  $\Phi$ -factory for nice experiments) accelerator of the INFN-LNF provides collisions between positrons and electrons at the center of mass energy of the  $\phi$ -meson.  $K^-K^+$  pairs are produced by the  $\phi$  mesons decay nearly at-rest [ $BR(K^+K^-) = (48.9 \pm 0.5)\%$ ] with low momentum ( $\sim 127$  MeV/c), which is ideal either to study reactions of stopped kaons in various targets, or to explore the products of the low energy nuclear absorptions of  $K^-$ . The  $K^-K^+$  pairs are emitted almost back-to-back, allowing then to tag the  $K^-$  through the detection of a  $K^+$  in the opposite direction.

The KLOE detector consists of a cylindrical drift chamber (DC) [37] and a fine sampling lead-scintillating fibres calorimeter [38], all surrounded by a superconducting solenoid which provides an axial magnetic field of 0.52 T. The DC, centred around the interaction point of DAΦNE, is characterised by an inner radius of 0.25 m, an outer radius of 2 m and a length of 3.3 m. The geometry of the detector provides a  $\sim 4\pi$  solid angle coverage and an acceptance of  $\sim 98\%$ . Tracks in the chamber are reconstructed with position and momentum resolutions of:  $\sigma_{R\phi} \sim 200$   $\mu\text{m}$  in the transverse  $R - \phi$  plane;  $\sigma_z \sim 2$  mm along the  $z$ -axis; the transverse momentum resolution for low momentum tracks ( $(50 < p < 300)$  MeV/c) is  $\frac{\sigma_{pT}}{pT} \sim 0.4\%$ .

The KLOE calorimeter is composed of a cylindrical barrel and two endcaps, providing a solid angle coverage of 98%. The volume ratio (lead/fibres/glue = 42:48:10) is optimised for a high light yield and a high efficiency for photons in the range (20–300) MeV/c. The photon detection efficiency is 99% for energies larger than 80 MeV and it falls to 80% at 20 MeV due to the cutoff introduced by the readout threshold. The position of the clusters along the fibres can be obtained with a resolution  $\sigma_{\parallel} \sim 1.4$  cm/ $\sqrt{E(\text{GeV})}$ . The resolution in the orthogonal direction is  $\sigma_{\perp} \sim 1.3$  cm. The energy and time resolutions for photon clusters are given by  $\frac{\sigma_E}{E_\gamma} = \frac{0.057}{\sqrt{E_\gamma(\text{GeV})}}$  and  $\sigma_t = \frac{57 \text{ ps}}{\sqrt{E_\gamma(\text{GeV})}} \oplus 100$  ps respectively.

The AMADEUS collaboration is presently analysing the data collected by KLOE during the 2004/2005 data taking. The statistics of the data sample corresponds to a total integrated luminosity of  $1.74 \text{ fb}^{-1}$ . The absorptions of the  $K^-$  in the materials of the detector setup, used as active target, are investigated. The DC entrance wall is composed of carbon fibre (750  $\mu\text{m}$ ) and Aluminium foil (150  $\mu\text{m}$ ). The percentage of  $K^-$  absorptions in carbon and aluminium was estimated by means of a dedicated GEANT Monte Carlo (MC) simulations of the KLOE apparatus (GEANFI [39]) using the GEISHA package to treat the  $K^-$  absorption physics. Out of the total fraction of captured kaons, about 81% is absorbed in the carbon fibre component and the residual 19% in the Aluminium foil. The KLOE DC is filled with a mixture of Helium and Isobutane (90% in volume  $^4\text{He}$  and 10%  $\text{C}_4\text{H}_{10}$ ). The analysed data include both  $K^-$  captures at-rest and in-flight. In the first case the negatively charged kaon is slowed down in the materials of the detector and consequently absorbed in a highly excited atomic orbit, from which it cascades down till it is absorbed by the nucleus as a consequence of the strong interaction. In the latter case the kaon penetrates the electronic cloud and interacts with the nucleus with an average momentum of about 100 MeV/c (due to energy losses in crossing the experimental apparatus).

## 3 Particle Identification and Events Selection

The events selection for the analyses presented in this paper starts with the identification of the  $\Lambda(1116)$  hyperon, which represents the signature of the  $K^-$  absorption process. The  $\Lambda$  is reconstructed from the charged decay into a proton and a  $\pi^-$  (the BR of the process is  $(63.9 \pm 0.5)\%$  [40]). Two tracks with opposite curvature in the DC and a minimum length of 30 cm are selected. The proton and pion identification is performed using the loss of energy ( $dE/dx$ ) information in the DC wires and the energy information provided by the calorimeter. In order to minimise the  $\pi^+$  contamination in the proton sample and to improve the purity of the particle identification, a minimum momentum of 170 MeV/c for the proton candidate is required. A common vertex is searched for all the  $p\pi^-$  pairs. Details about the reconstruction of the  $\Lambda$  decay vertex can be found in Ref. [1]. The mean value of the measured  $p\pi^-$  invariant mass distribution ( $m_{p\pi^-}$ ) is  $(1115.753 \pm 0.002)$  MeV/ $c^2$ , with a resolution of  $\sigma = 0.5$  MeV/ $c^2$ . A cut on the reconstructed invariant mass ( $1112 < m_{p\pi^-} < 1118$ ) MeV/ $c^2$  is applied.

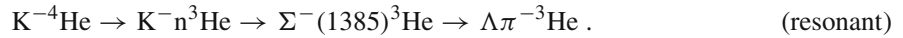
The second step of the events selection procedure consists in the identification of an extra-particle (a  $\pi^-$ , proton or triton), which is produced together with the  $\Lambda$  at the  $K^-$  hadronic interaction vertex. The vertex position is determined by backward extrapolating the  $\Lambda$  path and the extra-particle track. Particles momenta are corrected for energy loss. The distribution of the  $\Lambda\pi^-$ ,  $\Lambda p$ ,  $\Lambda t$  (hadronic) vertices along the radial direction ( $\rho$ ), orthogonal with respect to the DAΦNE beam pipe, is used to discriminate  $K^-$  hadronic absorptions on

the nuclei of the DC wall [the applied cut is  $\rho = (25.0 \pm 1.2)$  cm] from absorptions in the gas which fills the DC volume ( $\rho > 30$  cm).

#### 4 Modulus of the Non-resonant $K^-n \rightarrow \Lambda\pi^-$ Amplitude Below the $\bar{K}N$ Threshold

The  $K^-n$  single nucleon absorptions on  ${}^4\text{He}$  nuclei (the main component of the gas filling the DC), emitting a  $\Lambda$  and a  $\pi^-$  in the final state, are experimentally investigated in Ref. [29] by the AMADEUS collaboration. The aim is to extract information on the non-resonant ( $s$ -wave),  $I=1$ ,  $K^-n \rightarrow \Lambda\pi^-$  process. In this channel the non-resonant transition amplitude ( $|T_{K^-n \rightarrow \Lambda\pi^-}|$ ) can be extracted since the corresponding resonant counterpart, involving the formation of the  $\Sigma^-(1385)$  ( $I=1$ ), is well known. In  $K^-$  induced reactions the shape of the non-resonant hyperon-pion production in both  $I=1$  and  $I=0$  channels has to be experimentally disentangled in order to extract information on the  $\Lambda(1405)$ . The non-resonant  $\Sigma\pi$  production represents indeed the main bias in the interpretation of the measured spectra.

The elementary reactions, which give rise to the direct production of a  $\Lambda\pi^-$  pair in the final state of the  $K^-{}^4\text{He}$  absorption are:



In Ref. [41] it is argued that, when the  $K^-$  is absorbed at-rest on a neutron bound in  ${}^4\text{He}$ , the energy of the  $K^-n$  system is shifted by about 33 MeV below threshold. The energy shift is due to two main effects: (1) the binding energy of the absorbing nucleon (the neutron separation energy is  $B_n = 21$  MeV in  ${}^4\text{He}$ ); (2) the recoil energy of the  $K^-n$  pair with respect to the residual  ${}^3\text{He}$  (the average kinetic energy is of about 12 MeV).

The experimental  $\Lambda\pi^-$  invariant mass, momentum and angular distributions were simultaneously fitted in Ref. [29] with the corresponding distributions obtained from the MC simulation of the contributing processes, based on the phenomenological model described in Ref. [41]. The contributions of the at-rest/in-flight resonant and non-resonant  $K^-n \rightarrow \Lambda\pi^-$  direct productions in  ${}^4\text{He}$  were disentangled from the  $\Lambda\pi^-$  production following  $K^-$  absorptions on  ${}^{12}\text{C}$ , as well as from the non direct  $\Lambda\pi^-$  production, that is to say when a  $\Sigma$  hyperon is produced in the first step of the interaction, followed by the  $\Sigma N \rightarrow \Lambda N'$  conversion on the residual nucleons. The fit allowed to extrapolate the modulus of the non-resonant ( $s$ -wave)  $K^-n \rightarrow \Lambda\pi^-$  transition amplitude at  $(33 \pm 6)$  MeV below the  $\bar{K}N$  threshold, which is found to be:

$$|T_{K^-n \rightarrow \Lambda\pi^-}| = \left(0.334 \pm 0.018 \text{ (stat.)}_{-0.058}^{+0.034} \text{ (syst.)}\right) \text{ fm} . \quad (1)$$

In Fig. 1 the measured amplitude (with combined statistical and systematic errors) is compared with the theoretical predictions (see Refs: Barcelona (BCN) [23], Kyoto-Munich (KM) [24], Prague (P) [25], Murcia (M1 and M2) [26], Bonn (B2 and B4) [27]). For the BCN, KM and P models a theoretical uncertainty is quoted; for the other models the uncertainty is not available. This measurement should be used to test and constrain the  $s$ -wave  $K^-n \rightarrow \Lambda\pi^-$  transition amplitude calculations.

#### 5 $K^-$ Multi-Nucleon Absorption Branching Ratios and Cross Sections

The experimental investigation of the  $K^-$  2NA, 3NA and 4NA processes is performed in Ref. [34] exploiting  $K^-$  captures in  ${}^{12}\text{C}$  nuclei and reconstructing the  $\Lambda p$  pairs emitted in the final state of the reaction. The detected  $\Lambda$  hyperons are also produced in the decay of the  $\Sigma^0$  (i.e.  $\Sigma^0 \rightarrow \Lambda\gamma$ ) therefore, the  $K^-$  multi-nucleon absorptions in both  $\Lambda p$  and  $\Sigma^0 p$  final states are investigated.

The BRs and cross sections for the  $K^-$  2NA, 3NA and 4NA in the  $\Lambda p$  and  $\Sigma^0 p$  final states were extracted by means of a simultaneous fit of the  $\Lambda p$  invariant mass, angular correlation,  $\Lambda$  and proton momentum distributions with the corresponding MC distributions of the contributing processes. The simulations of the  $K^-$  nuclear captures at-rest and in-flight were based on the phenomenological model described in Refs. [41, 42]. In the case of  $K^-$  captures at-rest the absorption from the 2p atomic state was assumed. Fragmentations of the residual nucleus following the hadronic interaction were also considered. The fit allowed to disentangle three contributions for the  $K^-$  2NA:

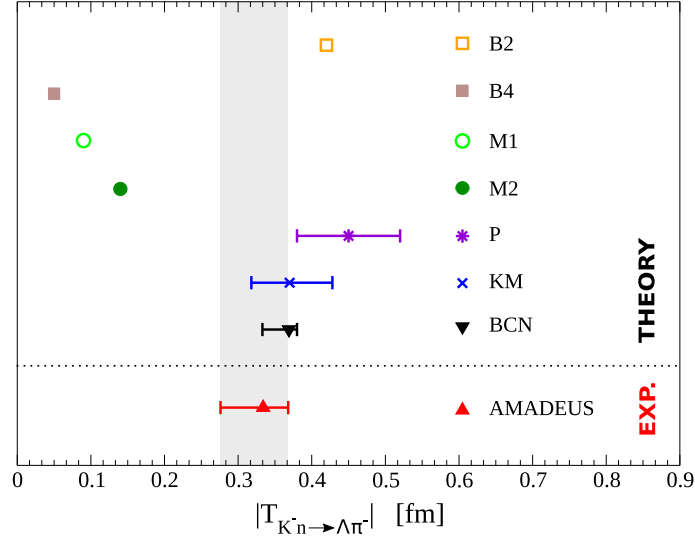


**Fig. 1** Modulus of the non-resonant transition amplitude for the  $K^-n \rightarrow \Lambda\pi^-$  process obtained by AMADEUS in Ref. [29], compared with theoretical predictions: Barcelona (BCN) [23], Kyoto-Munich (KM) [24], Prague (P) [25], Murcia (M1 and M2) [26], Bonn (B2 and B4) [27]

1. the Quasi-Free (QF) processes, in which the primarily produced  $\Lambda p$  and  $\Sigma^0 p$  pairs do not undergo final state interactions (FSIs) with the residual nucleus;
2. the primary  $\Lambda$  ( $\Sigma^0$ )N production followed by the elastic FSI processes (only single collisions of the hyperon and nucleon with the residual nucleus were considered);
3. the inelastic FSI processes, in which the primarily produced sigma particles convert into a  $\Lambda$  hyperon following the elementary reaction:  $\Sigma N \rightarrow \Lambda N'$ .

The measured BRs and low-energy cross sections of the distinct  $K^-$  2NA, 3NA and 4NA are reported in Fig. 2 (top and bottom panels respectively).

The global BR, obtained by summing the  $K^-$  2NA, 3NA and 4NA BRs (Fig. 2 top panel) is found to be

$$\text{BR}(\text{global}) = \left(21 \pm 3(\text{stat.})_{-6}^{+5}(\text{syst.})\right) \% , \quad (2)$$

which is in agreement with the  $K^-$  multi-nucleon absorption BRs in  $^4\text{He}$  and  $^{12}\text{C}$  measured in bubble chamber experiments [43,44]. The main contribution to the BR in Eq. (2) is given by the  $K^-$ 2NA-FSI and  $K^-$ 2NA-CONV  $\Sigma/\Lambda$  ratios.

In Ref. [45] it is demonstrated that the sum of the  $K^-$ 2NA BRs measured in Ref. [34] (also reported in Fig. 2 top panel) gives an estimate of the total BR of the  $K^-$ 2NA process in  $^{12}\text{C}$ . This is motivated by the fact that almost all the hyperon–nucleon combinations emerging as primary products of the  $K^-$ 2NA process contribute to the FSI and  $\Sigma/\Lambda$  conversion reactions in the measured  $\Lambda p$  final state (see Ref. [45] for the details). The sum of the  $K^-$ 2NA BRs measured in Ref. [34] is found to be

$$\text{BR}_{\Lambda p \text{ final state}}(K^-2NA \rightarrow YN) = \left(16.1 \pm 2.9(\text{stat.})_{-5.5}^{+4.3}(\text{syst.})\right) \% , \quad (3)$$

in agreement with the theoretical calculations (BCN model) given in Ref. [33] at  $0.3 \rho_0$  baryon density, which is the relevant density region for the absorption of low-energy  $K^-$  on  $^{12}\text{C}$  nuclei. Based on the measured BRs (Ref. [34]) and combining the theoretical/experimental information available in the literature (Refs. [33,44]) a missing contribution of  $(5.5 \pm 0.1(\text{stat.})_{-0.9}^{+1.0}(\text{syst.}))\%$  is found. Including the missing component, the total BR of the  $K^-$  2NA in carbon amounts to

$$\text{BR}(K^-2NA \rightarrow YN) = \left(21.6 \pm 2.9(\text{stat.})_{-5.6}^{+4.4}(\text{syst.})\right) \% . \quad (4)$$

Information on the in-medium dynamics of the antikaon–nucleon/nuclei interaction is provided by the ratio  $\mathcal{R}$  of the  $K^-$ 2NA-QF BRs in the  $\Lambda p$  and  $\Sigma^0 p$  channels. The BRs in Fig. 2 give

$$\mathcal{R} = \frac{\text{BR}(K^-pp \rightarrow \Lambda p)}{\text{BR}(K^-pp \rightarrow \Sigma^0 p)} = 0.7 \pm 0.2(\text{stat.})_{-0.3}^{+0.2}(\text{syst.}) \quad (5)$$

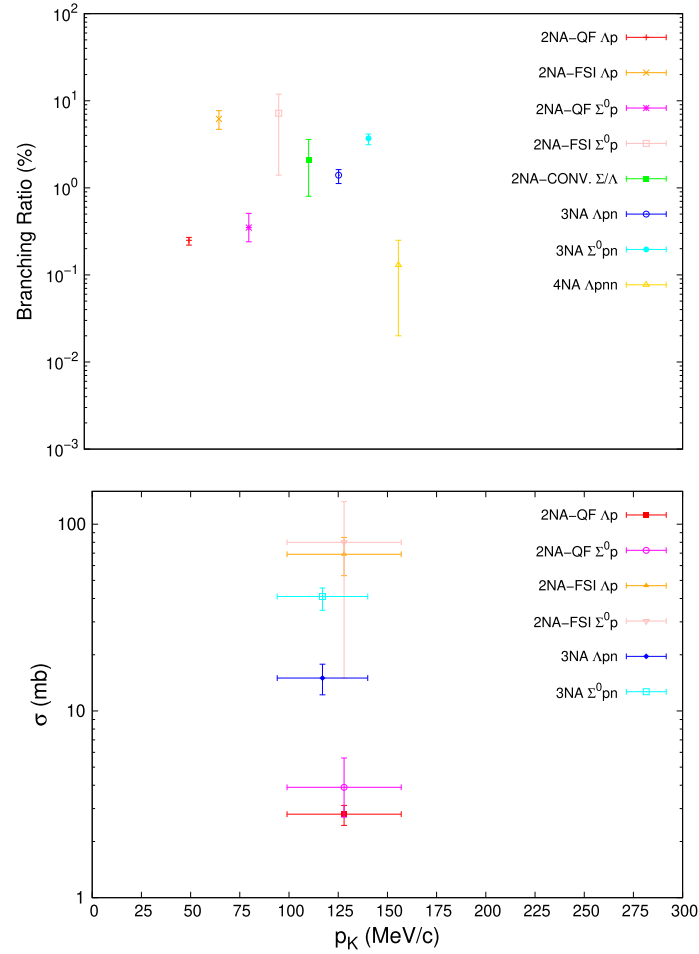


**Fig. 2** Branching ratios (top panel) and cross sections (bottom panel) of the  $K^-$  multi-nucleon absorption processes in  $^{12}\text{C}$ . The  $K^-$  momentum is evaluated in the centre of mass reference frame of the absorbing nucleons, thus it differs for the 2NA and 3NA processes

which indicates a dominance of the  $\Sigma^0 p$  final state. On contrary, by considering the ratio of the corresponding phase spaces ( $\mathcal{R}' = 1.22$ ) a dominance of the  $\Lambda p$  final state would be expected. The result in Eq. (5) was interpreted in Ref. [33] and was found to be in agreement with the theoretical calculations (BCN and P models) when the in medium effect due to the Pauli blocking is considered.

In Ref. [34] the contribution of a  $K^- pp$  bound state to the measured  $\Lambda p$  distributions was also investigated. It emerged that the  $K^- pp$  bound state signal completely overlaps with the  $K^- 2\text{NA-QF}$  contribution, the two components can be disentangled only for narrow states ( $\Gamma < 15 \text{ MeV}/c^2$ ) which are excluded by the theoretical calculations. A comparison with the FINUDA measurement [8] was performed as well by applying the same back-to-back  $\Lambda p$  events selection criterion used in Ref. [8] (i.e.  $\cos \theta_{\Lambda p} < -0.8$ ). The invariant mass distribution is compatible with the shape presented in Ref. [8]. The obtained spectra are completely described in terms of  $K^-$  multi-nucleon absorption processes, with no need of a  $K^- pp$  component in the fit, and the extracted BRs are in agreement with those obtained from the fit of the full data sample.

In Ref. [34] the contribution of the  $K^- 4\text{NA}$  was obtained with lower accuracy—with respect to the other disentangled multi-nucleon absorption processes - due to the overlap with the 3NA over a broad range of the phase space (compare for example the invariant mass distributions in Fig. 4 of Ref. [34]); moreover the  $\Lambda p$  production in  $K^- 4\text{NA}$  process is strongly uncorrelated.

The golden channel for the extrapolation of the  $K^- 4\text{NA}$  BRs and cross sections is represented by the  $K^- 4\text{NA} \rightarrow \Lambda t$  reaction, which is presently under investigation by the AMADEUS collaboration by using samples of both  $K^-$  captures on  $^4\text{He}$  and  $^{12}\text{C}$ . The investigation of the  $\Lambda t$  production in the final state of the  $K^-$  induced reaction on  $^6,^7\text{Li}$  and  $^9\text{Be}$  was previously performed in Refs. [46,47] where only global yields were

obtained, which include not only 4NA but also the dominant single nucleon absorption, FSI and conversion processes. Moreover, in Ref. [46] the selected events were found to be kinematically compatible with both  $\Lambda t$  and  $\Lambda dn$  production.

The key events selection criterion in the analysis performed by AMADEUS consists in the triton identification, which is performed by measuring the mass by time of flight. This allows to select a pure sample of  $\Lambda t$  events (see Ref. [36]). A simultaneous fit of the measured  $\Lambda t$  invariant mass, angular correlation and  $\Lambda t$  momentum to the MC simulated distributions of all contributing processes is performed, with the aim to extract the BRs and cross sections at  $p_K \simeq 100$  MeV/c for both  $K^-$  4NA in  ${}^4\text{He}$  and  ${}^{12}\text{C}$ .

## 6 Conclusions

In this paper, the results obtained by the AMADEUS collaboration from the analyses of the  $\Lambda\pi^-$ ,  $\Lambda p$  and  $\Lambda t$  correlated production in low-energy  $K^-$  absorptions on  ${}^4\text{He}$  and  ${}^{12}\text{C}$  nuclei were reviewed.

The modulus of the non-resonant ( $s$ -wave)  $K^-n \rightarrow \Lambda\pi^-$  scattering amplitude at  $\sqrt{s} = (33 \pm 6)$  MeV below the  $\bar{K}N$  threshold was extracted exploiting the  $K^-n$  single nucleon absorptions on  ${}^4\text{He}$  nuclei and amounts to  $|T_{K^-n \rightarrow \Lambda\pi^-}| = (0.334 \pm 0.018 \text{ (stat.)}_{-0.058}^{+0.034} \text{ (syst.)})$  fm. This measurement represents the first experimental constraint to the theoretical calculations of the  $s$ -wave  $K^-n$  scattering amplitude in the energy region below the  $\bar{K}N$  threshold. Moreover, the study of the spectral shape and of the yield of the non-resonant hyperon-pion production in  $K^-$  induced reactions serves as a reference in the experimental investigation of the  $\Lambda(1405)$  properties.

The measurement of branching ratios (BRs) and low-energy cross sections of the  $K^-$  multi-nucleon absorptions on two, three and four nucleons (2NA, 3NA and 4NA) was performed by reconstructing  $\Lambda p$  pairs emitted in the final state of  $K^-$  captures on  ${}^{12}\text{C}$ . A more accurate measurement of the  $K^-$  4NA contribution is presently ongoing by investigating the correlated production of a  $\Lambda$  and a triton in the final state of  $K^-$  absorptions on  ${}^4\text{He}$  and  ${}^{12}\text{C}$  nuclei. The measured BRs and low-energy cross sections of the distinct  $K^-$  2NA, 3NA and 4NA represent useful tests for the existing microscopical models of the  $K^-NN$  interaction and for future generalisation of  $K^-$  absorption models involving also more than two nucleons. Furthermore, in the light of the investigation of the low-energy capture of  $K^-$  on  ${}^{12}\text{C}$  target, no evidence emerges for  $K^-pp$  bound state formation. According to the phenomenological approach adopted for the interpretation of the data, such low-energy  $K^-{}^{12}\text{C}$  interaction is totally dominated by the nuclear form factor leaving no space for bound state evidence. Peculiar kaon momentum/target conditions still leave space to its existence (see Refs. [16, 18, 48, 49]). Our studies also show that DAΦNE is an ideal environment to study low-energy strangeness physics and we are presently considering new experimental proposals.

**Acknowledgements** We acknowledge the KLOE/KLOE-2 Collaboration for their support and for having provided us with the data and the tools to perform the analysis presented in this paper. Part of this work was supported by Ministero degli Affari Esteri e della Cooperazione Internazionale, Direzione Generale per la Promozione del Sistema Paese (MAECI), Strange Matter project PRG00892; EU STRONG-2020 project (Grant Agreement No. 824093); Polish National Science Center through Grant No. UMO-2016/21/D/ST2/01155.

## References

1. C. Curceanu et al., AMADEUS. *Acta Phys. Polon. B* **46**(1), 203–215 (2015)
2. A. Gallo et al., *Conf. Proc.* **C060626**, 604 (2006)
3. F. Bossi et al., *Riv. Nuovo Cim.* **31**, 531 (2008)
4. G. Agakishiev et al., HADES. *Phys. Rev. C* **87**, 025201 (2013)
5. J.C. Nacher, E. Oset, H. Toki, A. Ramos, *Phys. Lett. B* **455**, 55–61 (1999)
6. L. Tolos, L. Fabbietti, *Prog. Part. Nucl. Phys.* **112**, 103770 (2020)
7. J. Adamczewski-Musch et al., HADES. *Phys. Rev. Lett.* **123**(2), 022002 (2012)
8. M. Agnello et al., *Phys. Rev. Lett.* **94**, 212303 (2005)
9. G. Bendiscioli, A. Fontana, L. Lavezzi, A. Panzarasa, A. Rotondi, T. Bressani, *Nucl. Phys. A* **789**, 222–242 (2007)
10. T. Suzuki et al., KEK-PS E549. *Mod. Phys. Lett. A* **23**, 2520–2523 (2008)
11. T. Yamazaki et al., *Phys. Rev. Lett.* **104**, 132502 (2010)
12. A.O. Tokiyasu et al., LEPs. *Phys. Lett. B* **728**, 616–621 (2014)
13. G. Agakishiev et al., HADES. *Phys. Lett. B* **742**, 242–248 (2015)
14. Y. Ichikawa et al., *PTEP* **2015**(2), 021D01 (2015)
15. O. Vazques Doce, L. Fabbietti et al., *Phys. Lett. B* **758**, 134 (2016)
16. Y. Sada et al., J-PARC E15. *PTEP* **2016**(5), 051D01 (2016)

17. R. Münzer, L. Fabbietti, E. Epple, S. Lu, P. Klose et al., *Phys. Lett. B* **785**, 574–580 (2018)
18. S. Ajimura et al., J-PARC E15. *Phys. Lett. B* **789**, 620–625 (2019)
19. Y. Akaishi, T. Yamazaki, *Phys. Rev. C* **65**, 044005 (2002)
20. L.R. Staronski, S. Wycech, *J. Phys. G Nucl. Phys.* **13**(11), 1361 (1987)
21. J.A. Oller, U.G. Meissner, *Phys. Lett. B* **500**, 263–272 (2001)
22. D. Jido, J.A. Oller, E. Oset, A. Ramos, U.G. Meissner, *Nucl. Phys. A* **725**, 181–200 (2003)
23. A. Feijoo, V. Magas, A. Ramos, *Phys. Rev. C* **99**(3), 035211 (2019)
24. Y. Ikeda, T. Hyodo, W. Weise, *Nucl. Phys. A* **881**, 98 (2012)
25. A. Cieplý, J. Smejkal, *Nucl. Phys. A* **881**, 115 (2012)
26. Z.H. Guo, J.A. Oller, *Phys. Rev. C* **87**, 035202 (2013)
27. M. Mai, U.G. Meißner, *Eur. Phys. J. A* **51**, 30 (2015)
28. S. Acharya et al., ALICE. *Phys. Rev. Lett.* **124**(9), 092301 (2020)
29. K. Piscicchia, S. Wycech, L. Fabbietti et al., *Phys. Lett. B* **782**, 339 (2018)
30. E. Friedman, A. Gal, *Nucl. Phys. A* **959**, 66–82 (2017)
31. J. Hrtánková, J. Mareš, *Phys. Rev. C* **96**, 015205 (2017)
32. T. Sekihara, D. Jido, Y. Kanada-En'yo, *Phys. Rev. C* **79**, 062201 (2009)
33. J. Hrtánková, A. Ramos, *Phys. Rev. C* **101**(3), 035204 (2020)
34. R. Del Grande, K. Piscicchia, O. Vazquez Doce et al., *Eur. Phys. J. C* **79**(3), 190 (2019)
35. M. Agnello, FINUDA. *Phys. Rev. C* **92**(4), 92 (2015)
36. K. Piscicchia et al., *EPJ Web Conf.* **137**, 09005 (2017)
37. M. Adinolfi et al., *Nucl. Instrum. Methods A* **488**, 51–73 (2002)
38. M. Adinolfi et al., *Nucl. Instrum. Methods A* **482**, 364–386 (2002)
39. F. Ambrosino et al., *Nucl. Instrum. Methods A* **534**, 403–433 (2004)
40. M. Tanabashi et al., Particle data group. *Phys. Rev. D* **98**, 030001 (2018)
41. K. Piscicchia, S. Wycech, C. Curceanu, *Nucl. Phys. A* **954**, 75 (2016)
42. R. Del Grande, K. Piscicchia, S. Wycech, *Acta Phys. Pol. B* **48**, 1881 (2017)
43. P.A. Katz et al., *Phys. Rev. D* **1**(5), 1267 (1970)
44. C. Vander Velde-Wilquet, *II Nuovo Cimento A* (1965–1970) **39**, 538 (1977)
45. R. Del Grande, K. Piscicchia et al., *Phys. Scripta* **95**(8), 084012 (2020)
46. R. Roosen, J.H. Wickens, *II Nuovo Cimento A Ser. 11* **66**(1), 101 (1981)
47. M. Agnello et al., *Phys. Lett. B* **669**, 229 (2008)
48. T. Sekihara, E. Oset, A. Ramos, *PTEP* **2016**(12), 123D03 (2016)
49. T. Sekihara, E. Oset, A. Ramos, *J.P.S. Conf. Proc.* **26**, 023009 (2019)